Journal of Nuclear Materials 467 (2015) 357–367

Contents lists available at ScienceDirect

Journal of Nuclear Materials

journal homepage: www.elsevier.com/locate/jnucmat

The influence of microstructure on blistering and bubble formation by He ion irradiation in Al alloys

S.R. Soria [a, b, *], A. Tolley [a, b], E.A. Sánchez [a, b]

[a] Centro Atómico Bariloche, CNEA, Av. Bustillo 9500, 8400 S. C. de Bariloche, Argentina
[b] CONICET, Argentina

HIGHLIGHTS

- In Al and Al–4Cu, He bubbles were formed, but no bubbles were observed in Al-5.6Cu-0.5Si-0.5Ge.
- Bubble formation was enhanced at incoherent matrix/precipitate interfaces in Al–4Cu.
- The bubble size was insensitive to displacement rate in pure Al.
- In Al and Al-5.6Cu-0.5Si-0.5Ge blistering was observed, which was more severe in the alloy.
- Blistering effects were enhanced by increasing the displacement rate in Al and Al–4Cu.

ARTICLE INFO

Article history:
Received 19 March 2015
Received in revised form
18 September 2015
Accepted 29 September 2015
Available online 9 October 2015

ABSTRACT

The influence of microstructure and composition on the effects of ion irradiation in Al alloys was studied combining Atomic Force Microscopy, Scanning Electron Microscopy and Transmission Electron Microscopy. For this purpose, irradiation experiments with 20 keV He^+ ions at room temperature were carried out in Al, an Al–4Cu (wt%) supersaturated solid solution, and an Al-5.6Cu-0.5Si-0.5Ge (wt.%) alloy with a very high density of precipitates, and the results were compared. In Al and Al–4Cu, He bubbles were found with an average size in between 1 nm and 2 nm that was independent of fluence. The critical fluence for bubble formation was higher in Al–4Cu than in Al. He bubbles were also observed below the critical fluence after post irradiation annealing in Al–4Cu. The incoherent interfaces between the equilibrium θ phase and the Al matrix were found to be favorable sites for the formation of He bubbles. Instead, no bubbles were observed in the precipitate rich Al-5.6Cu-0.5Si-0.5Ge alloy. In all alloys, blistering was observed, leading to surface erosion by exfoliation. The blistering effects were more severe in the Al-5.6Cu-0.5Si-0.5Ge alloy, and they were enhanced by increasing the fluence rate.

1. Introduction

Materials in fusion reactors are subject not only to a flux of high energy neutrons, but also to the accumulation of He, that has a very low solubility in metals, through (n,α) reactions and through the decay of tritium [1]. Accumulation of He in metals is responsible for several effects that include void swelling by stabilization of vacancy clusters, formation of bubbles and surface erosion by blistering. At high irradiation temperatures, He accumulation leads to a progressive decay in the mechanical properties, causing embrittlement [2]. For these reasons, a detailed knowledge of the influence of He incorporation in structural materials for reactors is of fundamental importance to guarantee their safe operation.

The kind of defects that He produces in materials is strongly influenced by their microstructure and composition [3]. For example, in 316 steel, He bubbles form along grain boundaries, causing loss of ductility [4]. In Oxide Dispersion Strengthened steels, which contain a fine dispersion of oxide particles within the matrix, void swelling is dramatically reduced due to the high density of interfaces that represent sinks for He atoms [5].

Although Al is not a candidate material for fusion reactors, it is a model system in which the effects of ion irradiation have been extensively studied by many authors [6–8]. Two different effects were mainly reported: large scale blistering and the formation of nanometer sized bubbles. Blister evolution was shown to be

* Corresponding author. Centro Atómico Bariloche, CNEA, Av. Bustillo 9500, 8400 S. C. de Bariloche, Argentina.
E-mail addresses: sergiorsoria@gmail.com, sergio.soria@ib.edu.ar (S.R. Soria).

http://dx.doi.org/10.1016/j.jnucmat.2015.09.051
0022-3115/

strongly dependent on fluence. A critical fluence is necessary to initiate the formation of blisters, and beyond such critical fluence, blisters grow, coalesce and eventually burst, leading to exfoliation. Instead, bubble size was found to be largely unaffected by fluence.

Age hardenable Al alloys exhibit a wide variety of microstructures, depending on composition and thermomechanical treatment. They are therefore adequate to study the influence of microstructure on the effects of He ion implantation. For example, a correlation between He bubbles and precipitation processes was found in Al thin foils implanted with Cu and He ions [9]. However, the effects of He ion irradiation in Al alloys have received little attention.

In this work, the influence of composition and microstructure on He bubble formation and blistering due to He ion irradiation is studied combining Atomic Force Microscopy, Scanning Electron Microscopy and Transmission Electron Microscopy. The effects in pure Al are compared with those in an Al–4Cu (wt.%) supersaturated solid solution and an Al-5.6Cu-0.5Si-0.5Ge (wt.%) alloy containing a very high density of precipitates within the Al matrix.

2. Experimental

Specimens for irradiation experiments were prepared from pure Al, Al–4Cu and Al-5.6Cu-0.5Si-1.3Ge (wt.%) alloys. The alloys were prepared using 99.999% Al, 99.99%Cu, 99.99%Si and 99.99%Ge. Master alloys of Al–Cu, Al–Si and Al–Ge were prepared by induction welding. The alloys with the final composition were prepared by arc welding from the master alloys with the appropriate additions of pure Al.

The alloys were homogenized in sealed vycor tubes with Ar gas for 48 h at 773 K followed by water quenching. In Al–4Cu, this treatment resulted in a supersaturated solid solution. In Al-5.6Cu-0.5Si-1.3Ge, a subsequent ageing treatment of 3 h at 463 K was carried out in order to produce a dense distribution of nanometer sized Si–Ge and Al_2Cu θ' precipitates [10].

Slices with a thickness of 1 mm were cut with a low speed diamond saw, from which disc shaped specimens with 3 mm diameter were extracted by spark erosion. The thickness of the discs was reduced to 0.2 mm by mechanical grinding with 600 grit emery paper. In order to eliminate the damage caused by grinding, the surface to be irradiated was electropolished using a TENUPOL 5 unit, operating with a single jet, with an electrolyte containing 8% sulfuric acid, 2% hydrofluoric acid, 5% glycerol and 85% methanol (vol%). The applied voltage was 20 V and the polishing temperature was around 243 K. A surface roughness of 0.8 nm was determined in a 1 μm × 1 μm area with Atomic Force Microscopy, showing that the damage from mechanical grinding was effectively removed.

Ion irradiations were performed with 20 keV He ions at room temperature and normal incidence, at the 120 keV ion accelerator "Kevatrito" at Centro Atómico Bariloche. The experiments were carried out using beam current densities in the range of 1.9–3.5 μA cm^{-2} and 5–6 μA cm^{-2}, referred in the following to as "low beam current" and "high beam current", respectively. The displacement cross section was determined using the TRIM code [11]. The distribution of ion ranges and atomic displacements are shown in Fig. 1. From these simulations, an average displacement cross section of $\sigma_D = 5.8 \times 10^{-17}$ cm^2.ion^{-1} was obtained within a depth of 250 nm. Using this value, a fluence of 1.72×10^{16} ions.cm^{-2} corresponds to a damage of 1 displacement per atom. In the following, the number of displacements per atom (dpa) within a depth of 250 nm will be used as a measure of damage and will be referred to as "volume damage". Irradiations were carried out to volume damages of 1 dpa, 3 dpa, 7.5 dpa and 8.5 dpa, corresponding to fluences of 1.72×10^{16} ions.cm^{-2}, 5.16×10^{16} ions.cm^{-2}, 1.29×10^{17} ions.cm^{-2} and 1.46×10^{17} ions.cm^{-2}, respectively. However, in the region close to the specimen surface that is typically investigated by High Resolution Transmission Electron Microscopy (HRTEM), the displacement cross section is lower than the average value obtained above. From the simulation presented in Fig. 1, an average cross section of $\sigma_{DS} = 4 \times 10^{-17}$ cm^2.ion^{-1} for depths lower than 20 nm can be obtained. Therefore, when analyzing specimens irradiated to a given volume damage (in dpa), the number of displacements per atom in the region tested by HRTEM is 68% of the volume damage.

Surface characterization was carried out using an Autoprobe CP Atomic Force Microscope (AFM) from Park Scientific installed at the Atomic Collisions and Surface Physics Division in Centro Atómico Bariloche, using Ultralevers 0.6 μm silicon probes. Surface roughness was calculated from the topographic characterization as the root-mean-square deviation of the height distribution. An area of 2 μm × 2 μm was analyzed in all the specimens to allow comparison. These data were complemented with Scanning Electron Microscopy (SEM) images using secondary or backscattered electrons with a FEI NanoSEM230 at the Materials Characterization Division, Centro Atómico Bariloche.

Bulk characterization was carried out with Transmission Electron Microscopy (TEM) using a LaB_6 Philips CM200 microscope equipped with an Ultratwin lens, operated at 200 kV, at the Metals Physics Division in Centro Atómico Bariloche. The electron flux for high resolution imaging was estimated using the approximate relation between exposure time and electron current given by the microscope provider. A value of 6×10^{18} electrons.$cm^{-2}s^{-1}$was obtained. Using a displacement cross section of 100 b [12], the total displacements per atom can be kept below 0.1dpa if care is taken not to expose the area under observation more than about 2 min before capturing images.

3. Results

3.1. Low beam current effects

3.1.1. He ion irradiation on pure Al

Fig. 2 shows the AFM (panels A to D) and SEM (panels E to H) surface images as a function of increasing damage. After 1dpa, the AFM image (A) and its height distribution show the formation of small sized features with a surface roughness of 1.7 nm. The corresponding SEM image (E) shows the formation of blisters with a large size distribution, the smallest of which coincide with the features observed with AFM. The largest peak to valley height was about 9 nm. After 3dpa, the surface roughness was found to increase to 2.4 nm. A height profile analysis indicates blister growth and coalescence. The SEM image shows large blisters. The smaller blisters are not observed, probably due to improper focusing or to their very low height. Linear features observed at 3 dpa are attributed to preexisting defects in the specific specimens, that is, not caused by irradiation, since they were not observed at any other fluences. After 7.5 dpa, surface roughness increased strongly to 15.4 nm due to further blister growth. The SEM image shows that large blisters have begun to fracture leading to an exfoliation process. After 8.5 dpa, a marked reduction in surface roughness was measured with AFM and large features were observed with SEM. Combining the information from both techniques, the results are attributed to a significant exfoliation process in which large blisters burst and a second generation of small blisters begins to form.

The evolution of surface roughness with irradiation time or fluence (expressed in dpa) for pure Al is shown in Fig. 3, together with the results for the Al–5.6Cu–0.5Si–1.3Ge alloy that will be presented in the following section.

Characterization of the near surface bulk (thickness of the order of 20 nm) was carried out with TEM. No contrast due to dislocations

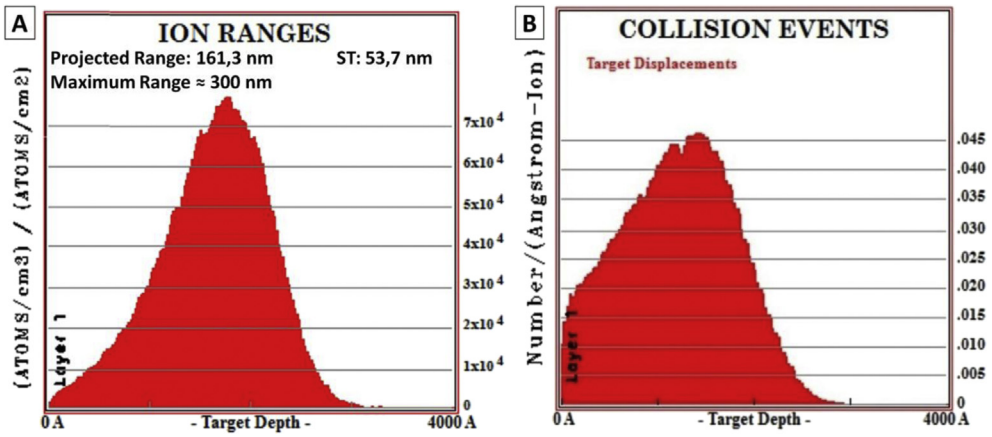

Fig. 1. Ion ranges (A) and collision events (B) as a function of depth obtained by TRIM [11] for implantation of 20 keV He^+ on Al at normal incidence.

or dislocation loops was observed when the specimen was imaged in dynamical 2-beam conditions. Instead small-sized bubbles were observed. Fig. 4 shows the characteristic contrast inversion observed in overfocussed and underfocussed images of nanometer sized bubbles in Al irradiated to a volume damage of 1 and 8.5 dpa (corresponding to near surface damage of 0.7 dpa and 5.8 dpa, respectively). The diameter of the observed bubbles, between 1 and 2 nm, was found to be unaffected by irradiation, up to the highest damage.

3.1.2. He ion irradiationonAl–5.6Cu–0.5Si–1.3Ge (wt.%)

Fig. 5 shows the AFM (A) and SEM (B) surface images and the TEM (C) bulk characterization before irradiation. Disc-shaped features with a diameter of a few hundreds of nm were observed with SEM, with a height difference with respect to the matrix of 2 nm, determined by AFM. Such features were brighter than the matrix in SEM images obtained with back scattered electrons. The observed morphology and size of such features indicate that they are precipitates of the equilibrium θ phase formed during the high temperature homogenization treatment. The microstructure determined by TEM showed a large density of precipitates with size of a few nanometers. Such defects are identified as Si–Ge rod-shaped precipitates, indicated with red arrows in Fig. 5, and edge-on disc-shaped metastable θ′ Al_2Cu precipitates, in accordance with the literature.

Fig. 6 shows the AFM (panels A to D) and SEM (panels E to H) surface images as a function of increasing damage. The evolution of surface roughness with irradiation time or fluence is shown in Fig. 3. After 1dpa, the surface roughness was 5.3 nm. The corresponding SEM (E) image shows dark features that correspond to blisters of about 150 nm in diameter. Peak to valley heights in the range of 15 nm–25 nm were measured. After 3 dpa, surface roughness increased to 8.7 nm. Large blisters with diameters up to 400 nm were observed. Some blisters exhibited cracks. After 7.5 dpa, surface roughness decreased slightly to 7.6 nm. Large scale heterogeneous blistering was observed with SEM, with a broad size distribution. Some blisters had diameters smaller than 1 μm while others were about 10 μm in diameter. Some blisters show cracks indicating the beginning of the exfoliation process. After 8.5 dpa, surface roughness was significantly reduced, to a value similar to that of unirradiated specimens. The SEM images after 7.5 dpa and 8.5 dpa were obtained with the specimen surface inclined 35° to the electron beam to improve visualization of blisters.

No bubbles were observed with TEM at all fluences. The thinned TEM specimens were subsequently annealed at 523 K for 5 h. However, bubbles were not observed after the heat treatment. This is illustrated in Fig. 7, in which a pair of overfocussed and underfocussed images are shown.

3.1.3. He ion irradiation on Al–4Cu (wt.%)

Specimens of an Al–4Cu solid solution were irradiated in the same conditions as the Al and Al-5.6Cu-0.5Si-1.3Ge alloys, and TEM characterization of the region near the irradiated surface was carried out. In specimens irradiated to a volume damage of 1 dpa, no contrast due to extended dislocations or dislocation loops was observed and, unlike pure Al, no nanometer sized bubbles were detected. However, after annealing treatments of 5 h at 473 K and 523 K, bubbles with mean diameters of 2 nm and 2.5 nm, respectively, were found. Images of such bubbles are shown in Fig. 8a-b. In these figures, contrast due to dislocations can also be seen. We assume that such dislocations were formed during manipulation of the thin foil specimen for the annealing treatment, since no dislocations had been observed immediately after the irradiation. During annealing, precipitates were also formed. In the very thin regions, large equilibrium θ phase precipitates were found while in the thicker regions, metastable θ′ and θ″ precipitates were also observed. At the θ/matrix interfaces, bubbles, with diameters up to 4.7 nm, were observed. Fig. 8c–d shows even larger bubbles, with diameters of 6 nm, located at the interface between two equilibrium θ phase precipitates. Such bubbles are assumed to form at the triple interface between the matrix and the two precipitates.

3.2. High beam current effects

High beam current experiments were carried out in Al and the Al–4Cu supersaturated solid solution. Blistering was so severe that it was difficult to obtain stable AFM images. Fig. 9 shows SEM images of Al and Al–4Cu obtained with the surface inclined 35° to the electron beam. After 3 dpa, it can be seen that blistering Al–4Cu (C, D) is more severe than in Al (A, B), and in turn, more severe than in Al irradiated with low beam current (see Fig. 2 B). In Al, after 3 dpa and 7.5 dpa, second generation blisters can be observed within first generation blisters that have bust and lost their caps. In addition, two kinds of exfoliation processes can be observed: one in which the blister cap is removed completely from the surface and another where the blister cap is only partly removed. Similar effects were observed in Al–4Cu after 3 dpa and 7.5 dpa. From the SEM images of burst blisters, the blister cap thickness was determined. A value

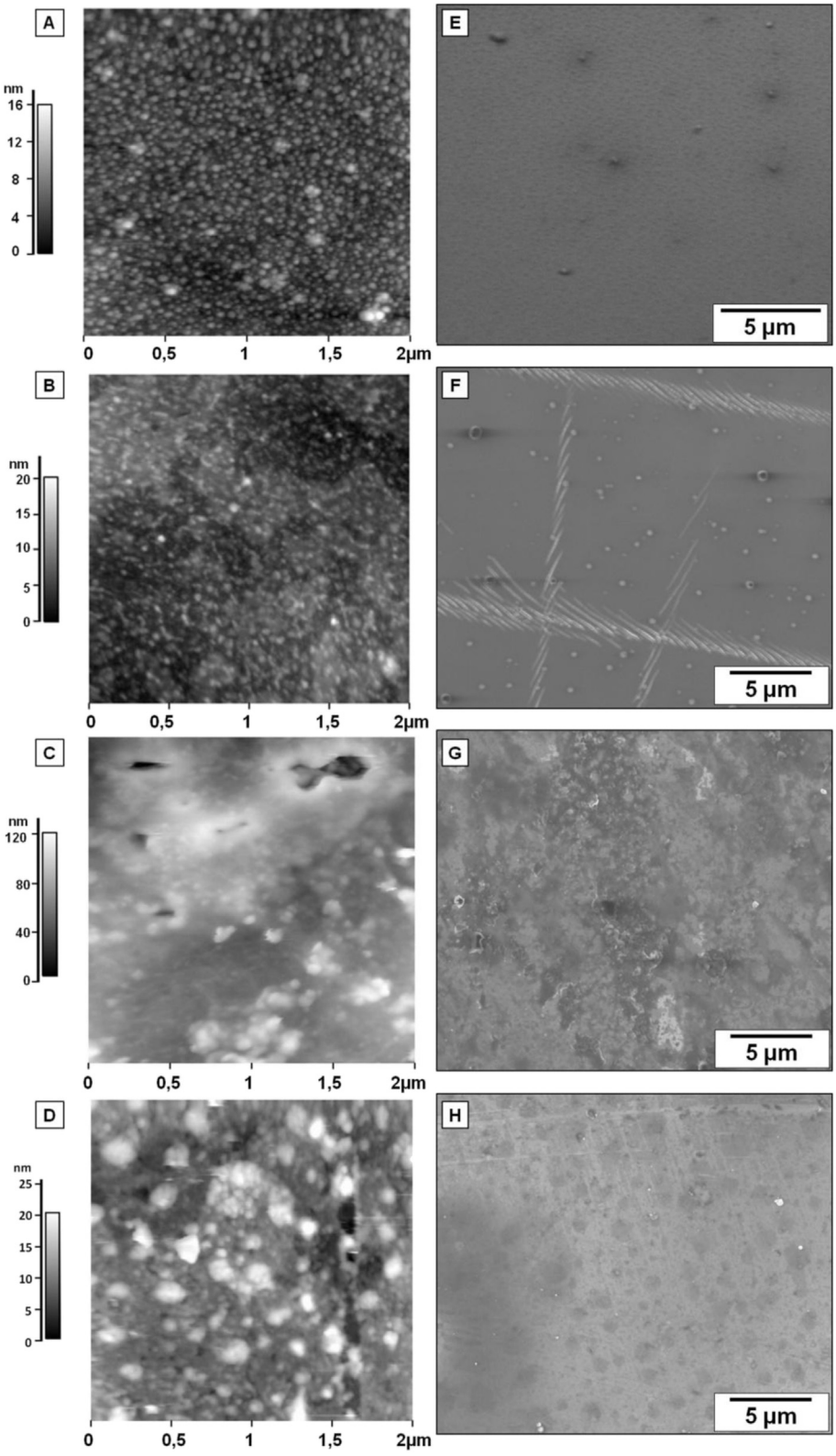

Fig. 2. AFM and SEM micrographs in pure Al after 1dpa (A, E), 3 dpa (B, F), 7.5 dpa (C, G) and 8.5 dpa (D, H) irradiation with 20 keV He^+ ions, respectively.

of 270 ± 30 nm was obtained that is 1.6 times longer than the projected length of the ions in the material (161 nm), and close to the maximum penetration depth (300 nm).

In both Al and Al–4Cu, small sized bubbles were observed directly after irradiation to volume damages of 3 and 7.5 dpa, without post irradiation annealing. The size was similar for both irradiations, and very similar to that determined in Al after low beam current irradiations. Fig. 10 illustrates the bubbles observed in

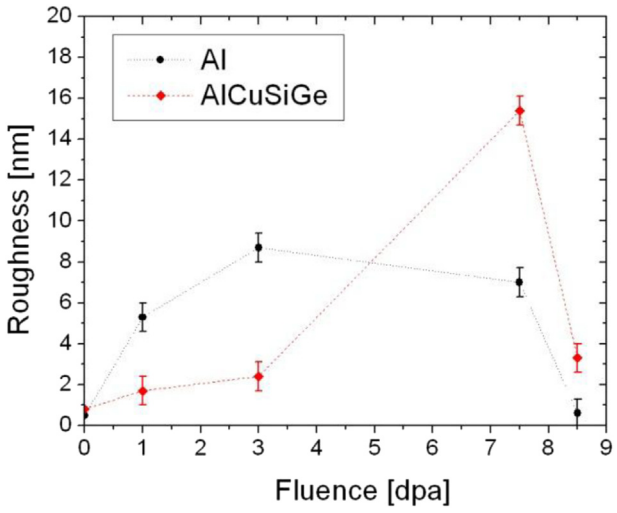

Fig. 3. Evolution of surface roughness with irradiation fluence (expressed in dpa) for pure Al and Al–5.6Cu–0.5Si–1.3Ge (wt.%).

Al–4Cu after a volume damage of 3 dpa, that corresponds to a damage of 2 dpa in the region analyzed by HRTEM.

4. Discussion

4.1. Bubble formation

He has a negligibly small solubility in metals, and therefore precipitates forming bubbles [13]. In Al, bubble formation due to He ion implantation has been studied by several authors [6–8]. The present results have shown the formation of bubbles with sizes in the range of 1–2 nm, and that the size was essentially unaffected by fluence. These results are in accordance with those reported by Ono et al. [14], where bubbles with a constant size of 1.5 nm were reported due to 20 keV He ion irradiation up to fluences in the range of 1×10^{13}–1×10^{16} ions.cm^{-2}.

The number of He atoms implanted during the irradiation experiments, N_I, was estimated using the following equation

$$N_I = \frac{\phi}{R} \tag{1}$$

that assumes that no He escapes the implanted region [15]. ϕ is the fluence and R is the projected range.

For a fluence equivalent to 1 dpa in pure Al, the density of implanted He atoms was 1×10^{21} ions.cm^{-3}.

The density of He atoms contained in bubbles, N_B, was calculated using Eq. (2)–(4), in which δ is the bubble density, n the number of He atoms per bubble, r_B the bubble radius, p the bubble pressure, V the atomic volume of He, T the absolute temperature and K_B the Boltzmann constant. To calculate V, the equation of state for rigid spheres of Carnahan and Starling [16] was used (Eq. (4)), with an atomic diameter d obtained using the modified Buckingham potential [17]. Considering that He bubbles were in equilibrium, the pressure p was calculated by using $p = 2\gamma/r_B$, where γ is the surface tension of Al (1 J/m^2) [18].

$$N_B = \delta \cdot n \tag{2}$$

$$n = \frac{4}{3} \cdot \pi \cdot \frac{r_b^3}{V} \tag{3}$$

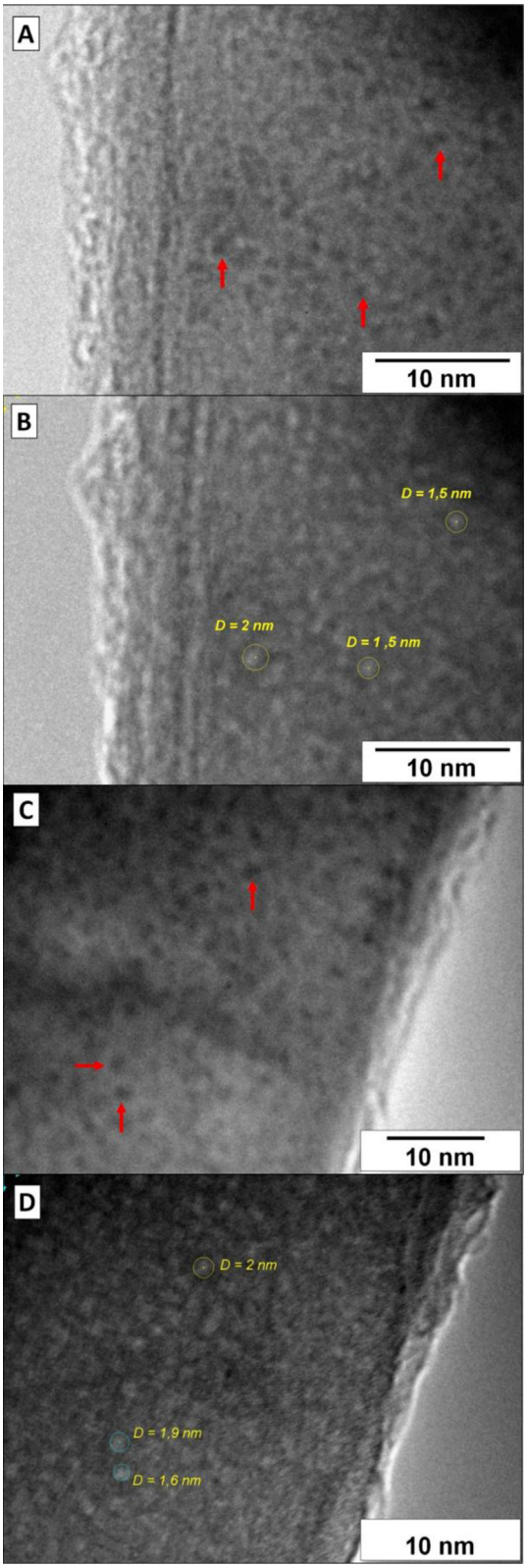

Fig. 4. He bubbles in pure Al after 1dpa (overfocussed (A) and underfocussed (B)) and 8.5 dpa (overfocussed (C) and underfocussed (D)) irradiation. Arrows refer to measured bubbles.

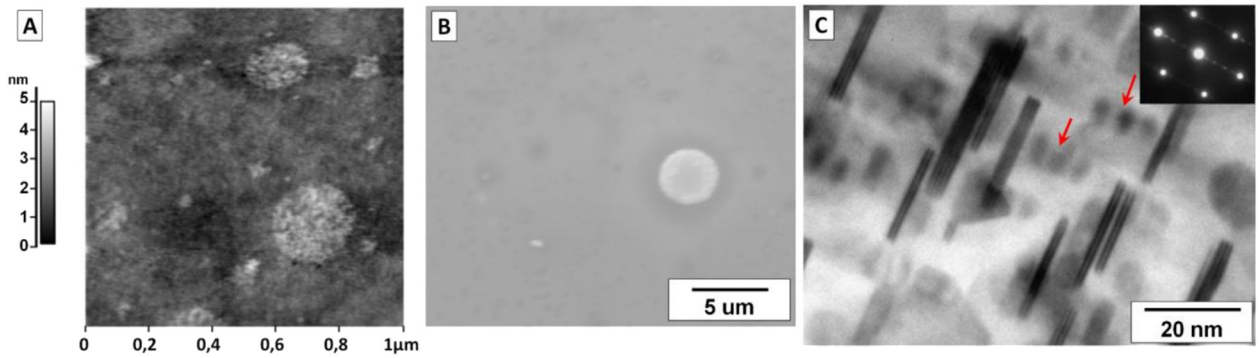

Fig. 5. AFM (A), SEM (B) and TEM (C) micrographs in Al–5.6Cu–0.5Si–1.3Ge (wt.%) alloy before irradiation. Large equilibrium θ phase precipitates can be observed in A and B. The TEM micrograph in C shows a high density of Si–Ge precipitates (indicated by arrows), and metastable θ′ precipitates.

$$\frac{p\cdot V}{K_B\cdot T}=\frac{(1+y+y^2-y^3)}{(1-y)^3}, y=\frac{\pi\cdot d^3}{6\cdot V} \quad (4)$$

Using the above equations with $r_B = 0.8$ nm and $\delta = 2.5 \times 10^{18}$ bubbles.cm^{-3} estimated from TEM images (26 bubbles were identified in an area of 16 nm × 22 nm, with an estimated thickness of 30 nm), the number of He atoms per bubble was $n = 158$, and the density of He atoms contained in bubbles was $N_B = 4 \times 10^{20}$ cm^{-3}, that is only a fraction of the total amount of He atoms implanted.

In Al–4Cu, bubbles were not observed after low beam current irradiation. This result indicates that the presence of Cu in solid solution inhibits bubble formation. A similar effect was reported in neutron irradiation experiments [19] in Al up to fluences corresponding to a damage of 2.6 dpa, where the addition of Cu in solid solution reduced void formation in the material. After post-irradiation annealing, however, bubbles were observed to form in the bulk, and larger sized bubbles were observed to form at the interfaces between the equilibrium θ phase and the matrix. Such interfaces are known to be incoherent, and, due to their high interfacial energy, could be adequate sites for heterogeneous nucleation of bubbles. Instead, no bubbles were observed on the interfaces between the matrix/θ″ or matrix/θ′ that are highly coherent or semicoherent, respectively.

No bubbles were observed after low current density irradiation in Al–Cu–Si–Ge with a high density of precipitates, neither in the bulk nor on matrix/precipitate interfaces, nor were any bubbles observed after post irradiation annealing. On one hand this result supports the conclusion from the previous section that the semi-coherent matrix/θ′ interfaces are not suitable heterogeneous nucleation sites. On the other hand this result suggests that the presence of a high density of precipitates inhibits bubble formation, even more effectively than Cu impurities in solid solution, since no bubbles were formed even after post-irradiation annealing. The precise mechanism by which Cu in solid solution or a dense distribution of precipitates inhibit bubble formation is not yet clear. It is important to point out that bubble formation involves not only He atoms but also vacancies. The presence of Cu in solid solution or that of precipitates may affect the mobility of vacancies of He atoms. Further results concerning bubble formation were obtained in high beam current experiments that will be discussed in section 4.3.

4.2. Blistering effects

In the previous section it was shown that only a small fraction of the implanted He atoms is contained in bubbles close to the specimen surface. Therefore, most of the implanted He contributes to the blistering process. Previously published results of He irradiation experiments in Cu and Si obtained in cross section specimens have shown that small bubbles are formed just below the irradiated surface, and as depth increases the bubbles' size is progressively larger [20,21], so that bubble size roughly follows the implantation profile as calculated using the TRIM code. At the depth corresponding to the maximum implantation concentration, bubbles coalesce forming large blisters. The present results that show the formation of small sized bubbles near the irradiated surface and large sized blisters can be understood in terms of the above mentioned papers.

In Al, surface roughness was found to increase with damage, up to 7.5 dpa. This was shown to be related to the formation, growth and coalescence of blisters. Between 7.5 dpa and 8.5 dpa a strong reduction of surface roughness was measured, and was shown to be related to an exfoliation process caused by the cracking of blisters and subsequent detachment of the lid. Similar results have been reported for Ar implantation in Si, where a second generation of Si, where a second generation of blisters was observed to occur within cracked blisters of the first generation [22].

Reduction of surface roughness could be also attributed to sputtering effects. However, according to the sputtering yield of 0.1 atoms per ion, determined with the TRIM code, the maximum surface erosion corresponding to the largest fluence amounts to 2.4 nm, that is much lower than the surface roughness reduction of 15 nm. Furthermore, sputtering effects would not account for the initial increase in surface roughness followed by an abrupt reduction, as the present results have shown (Fig. 2c).

In Al-5.6Cu-0.5Si-1.3Ge, the increase and the subsequent decrease of surface roughness occurs at lower fluences than in pure Al. These results, together with those obtained from AFM and SEM images, indicate that blister formation and growth, and the associated exfoliation process occur at lower fluences, and are more severe in Al-5.6Cu-0.5Si-0.5Ge than in pure Al. This behavior contrasts with that of bubble formation, as observed with TEM. For the case of the alloy, no bubbles were observed, whereas a high density of bubbles were formed in pure Al. Taking into account the results of Fig. 5, the main microstructural difference is that the alloy contains a high density of precipitates (rod-shaped Si–Ge and plate-shaped θ′ Al_2Cu) and a low density of θ phase precipitates; so, these precipitates should be responsible for the differences observed in bubble and blister formation.

The bubbles are produced by the accumulation of He in the voids produced by bulk atom displacements, but they can be reduced if a high density of interfaces acts as sinks for He atoms [5]. Therefore, the high density of Si–Ge and θ′ phase precipitates in the Al-5.6Cu-0.5Si-0.5Ge alloy, reduce the presence of bubbles in the bulk near the irradiated surface (as seen by TEM).

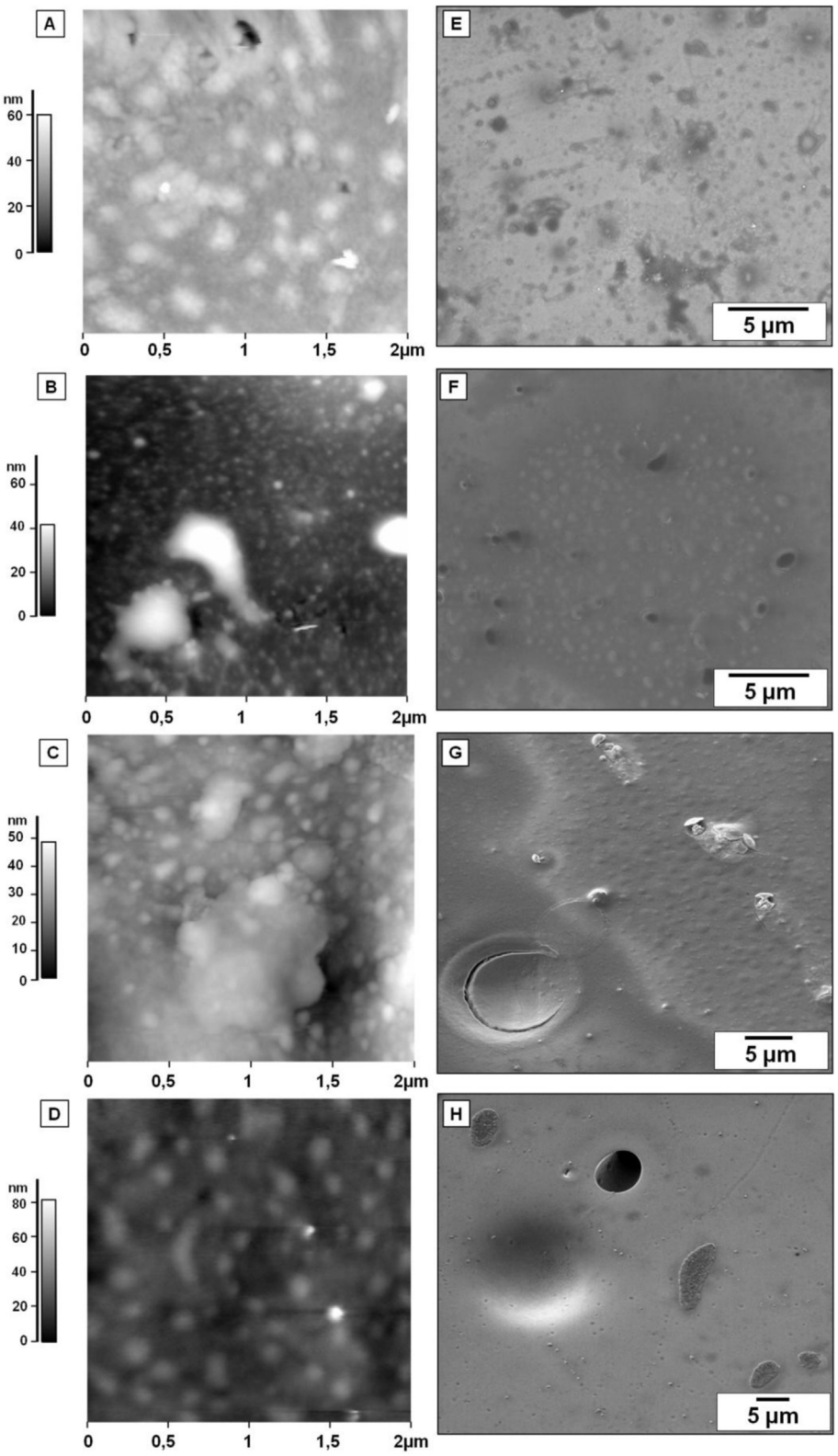

Fig. 6. AFM and SEM micrographs in Al–5.6Cu–0.5Si–1.3Ge (wt.%) alloy after 1dpa (A, E), 3 dpa (B, F), 7.5 dpa (C, G) and 8.5 dpa (D, H) irradiation with 20 keV He^+ ions, respectively.

On the other hand, in the deeper region of the sample where the damage is higher (depth of about 200 nm), the enhanced heterogeneous bubble nucleation at the incoherent matrix/θ phase interfaces stimulates the formation of fewer but larger blisters, thus reducing the critical fluence for the blistering process. This effect is not seen by TEM because it analyses the region close to the surface (~20 nm), but it is revealed at the surface by the distortion of the topography due to the inner pressure in the blister, as seen by SEM

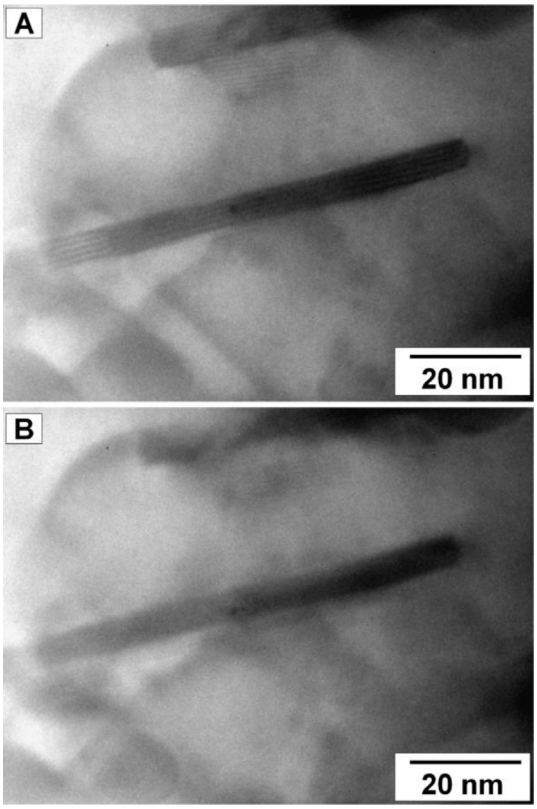

Fig. 7. TEM micrographs in Al–5.6Cu–0.5Si–1.3Ge (wt.%) alloy after 8.5 dpa and post-irradiation annealing at 250 °C for 5 h: focussed (A) and overfocussed (B).

and AFM. The observation that the distribution of blisters in Al-5.6Cu-0.5Si-0.5Ge was more inhomogeneous than in pure Al, supports the assumption that the formation of blisters is related to the coarse distribution of θ phase precipitates.

4.3. Displacement rate dependence of irradiation effects

In Al, high beam current irradiations resulted in more severe blistering for the same fluence as compared to low beam current experiments, indicating a displacement rate (current density) dependence of the blistering process. However, the bubble distribution and size were the same as in low beam current experiments, indicating that bubble formation was unaffected by the displacement rate increase. A displacement rate dependence of the blistering process has been reported for 500 keV He ion irradiations on V and Nb at 1173 K [3]. This effect was attributed to the competence between the rate of incoming He ions and the rate at which He atoms diffuse away from the region of implantation. Following this interpretation, increasing the displacement rate enhances blistering because the He atoms are implanted faster leading to a larger local supersaturation.

The measured value of blister wall thickness (270 ± 30 nm) was found to be larger than the projected range of the implanted He atoms simulated by the TRIM code, of 161 nm. A similar effect was observed in He ion irradiation experiments in pure aluminum with energies in the range of 10–80 keV [23], where the difference between the projected range and the blister wall thickness was attributed to swelling effect caused by the formation of bubbles. However, in the present results, the swelling effect can be estimated from the bubble volume fraction calculated from the density of bubbles determined by TEM, which is below 10%. In order to explain the difference of 110 nm between the measured blister cap thickness of 270 nm and the projected range of 161 nm, a swelling

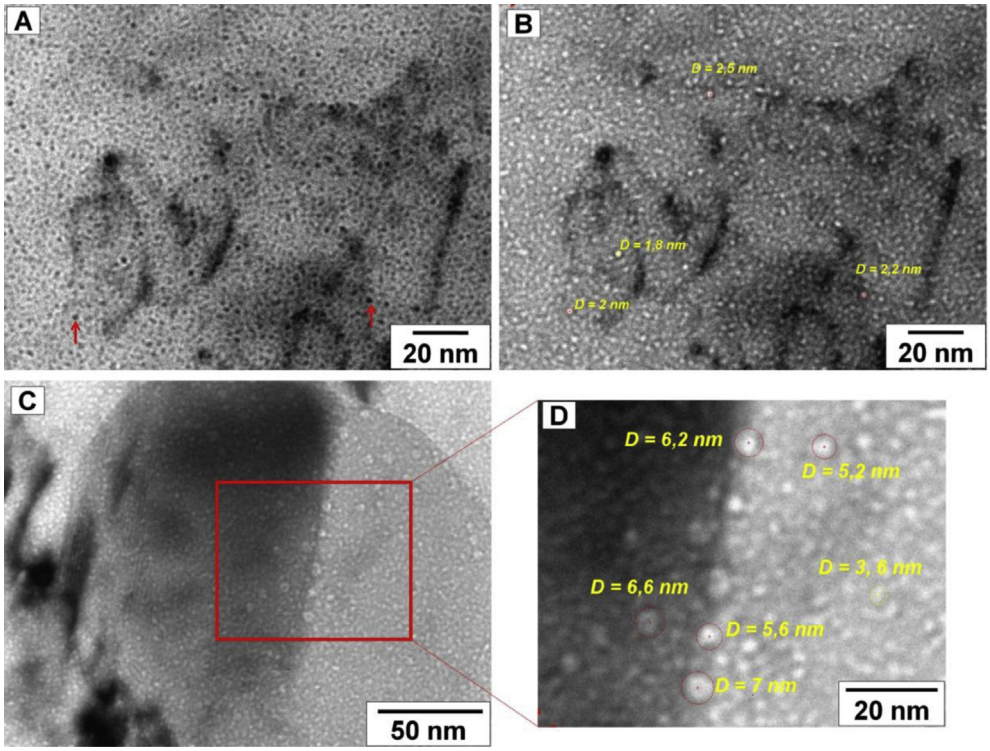

Fig. 8. He bubbles in Al–4Cu(wt.%) after 1 dpa and post-irradiation annealing at 200 °C for 5 h:underfocussed (A), overfocussed (B) and bubbles formation on matrix/θ precipitate interfaces, undefocussed micrographs (C, D). Arrows indicate measured bubbles.

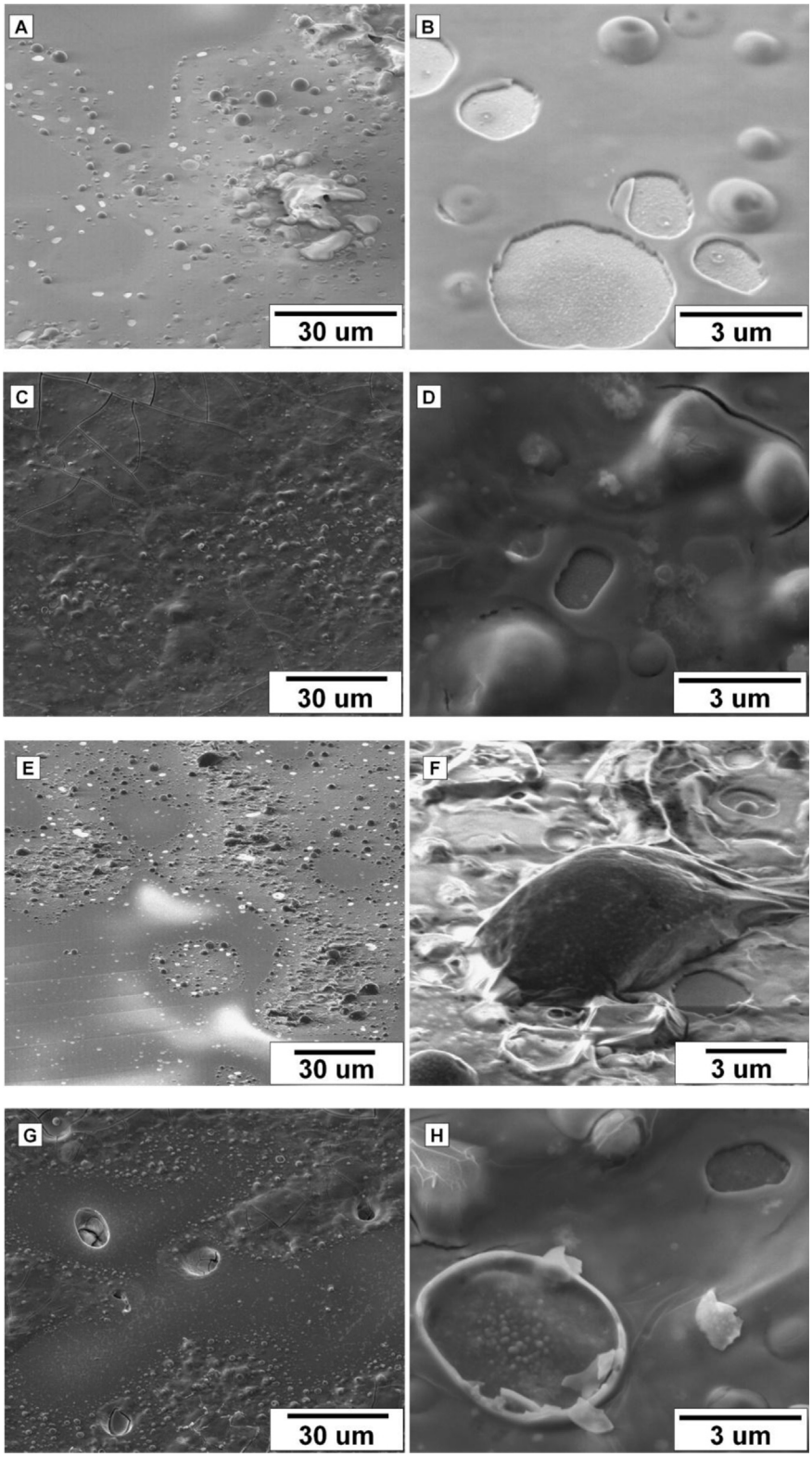

Fig. 9. SEM micrographs in pure Al after 3 dpa (A, B) and 7.5 dpa (E, F) and Al–4Cu(wt.%) alloy after 3 dpa (C, D) and 8.5 dpa (G, H), respectively.

effect of 70% is required. Therefore, the present results favor the lateral stress model proposed by Das et al. [24], in which the blister cap thickness is similar to the maximum penetration of implanted atoms. For 20 keV He irradiation, the maximum implanted depth corresponds to about 300 nm, in good agreement with the measured blister cap thickness.

For 3 dpa and 7.5 dpa a second generation of blisters was observed to form (Fig. 9 A, F). Similar multiple generation blistering effects have been reported after 40 keV He ion irradiation in Al to a fluence of 1×10^{18} ions.cm^{-2}, where up to six generation of blisters

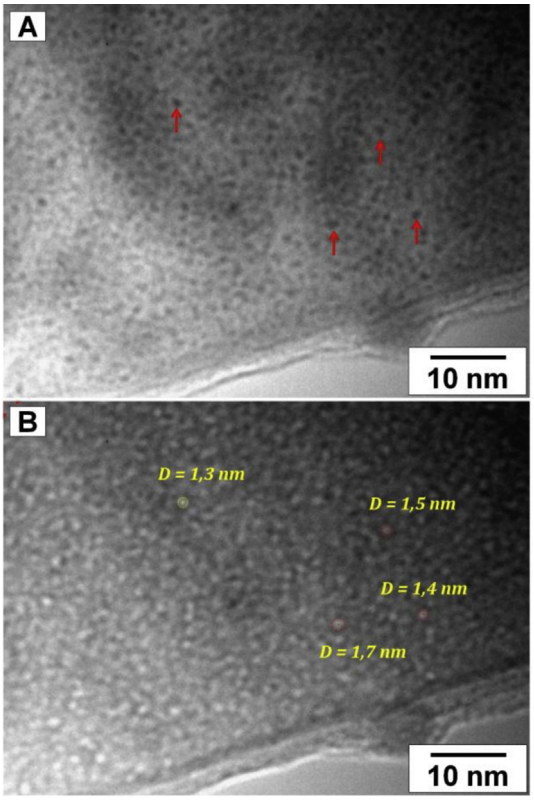

Fig. 10. He bubbles in Al–4Cu(wt.%) alloy after 3 dpa without post-irradiation annealing: underfocussed (A), overfocussed (B). Arrows indicate measured bubbles.

were observed [23].

In Al–4Cu irradiated with high beam current to 3 and 7.5 dpa, severe blistering was observed, that increased with fluence, and was stronger than that observed at lower beam current. Two generations of blisters were observed at both fluences. Bubbles were observed directly after irradiation without post irradiation annealing. This is in contrast to the results obtained at lower displacement rates, where no bubbles were observed directly after irradiation for fluences up to 1dpa. However, since in pure Al the displacement rate did not influence the formation of bubbles, the difference can be simply attributed to the fact that larger fluences were reached, and so the critical fluence for bubble formation was surpassed. According to this interpretation, the critical fluence for bubble formation in Al–4Cu is between 1 and 3 dpa, larger than that of pure Al, that is below 1 dpa. The mean bubble diameter of 1.5 nm was independent of fluence. This result agrees with previous reports in pure Al [15].

Finally, it is important to note that room temperature irradiation of the Al–4Cu supersaturated solid solution did not result in the formation of precipitates of the equilibrium θ phase, nor of metastable θ′ or θ″phases. Such precipitates could have been expected to form a consequence of irradiation induced enhanced diffusion.

5. Conclusions

The influence of composition, microstructure and displacement rate on the effects of room temperature ion irradiation in Al alloys using 20 keV He ions was studied. For this purpose, the effects in pure aluminum, a solid solution of Al–4Cu (wt.%) and an Al-5.6Cu-0.5Si-1.3Ge (wt.%) alloy with a very dense distribution of precipitates were compared.

From the analysis of the results, the following conclusions were reached:

1. In Al and Al–4Cu, He bubbles were formed above a critical fluence, with a uniform distribution and size in between 1 and 2 nm, independent of fluence.
2. The critical fluence for He bubble formation was higher in the Al–4Cu solid solution than in pure Al.
3. In Al–4Cu, below the critical fluence for bubble formation, He bubbles were formed by post irradiation annealing at 473 K. Larger sized bubbles were found at the interfaces between the matrix and the equilibrium θ phase that formed also during the post irradiation annealing. This effect was attributed to enhanced nucleation at the incoherent interfaces.
4. In Al–5.6Cu–0.5Si–1.3Ge, no bubbles were observed directly following irradiation or after post irradiation annealing at a temperature of 523 K. This effect was attributed to the trapping of He atoms at the coherent interfaces between the matrix and θ′ and Si–Ge precipitates.
5. In Al and Al–5.6Cu–0.5Si–1.3Ge, blistering was observed, that increased with fluence and led to surface erosion by exfoliation. The blister distribution was homogeneous in Al. Instead, in Al–5.6Cu–0.5Si–1.3Ge blistering was more severe than in Al for the same fluence, and the blister distribution was inhomogeneous. The enhanced blistering in Al–5.6Cu–0.5Si–1.3Ge was attributed to the presence of incoherent equilibrium θ phase precipitates formed during the homogenization process due to excess Cu.
6. Blistering effects were enhanced by increasing the displacement rate (current density) in Al and Al–4Cu.
7. The bubble size was insensitive to displacement rate in pure Al.
8. In the supersaturated Al–4Cu solid solution, neither equilibrium nor metastable precipitates were formed during irradiation.

Acknowledgments

The assistance of Dr. Oscar Grizzi during the irradiation experiments and of Mr. Carlos Cotaro for the SEM observations is gratefully acknowledged. S.R. Soria carried out this work with a fellowship of the Atomic Energy Commission. We also acknowledge partial support from ANPCyT (PICT 0643 and PICT 0124), CONICET (PIP 112-201101-00594) and Universidad Nacional de Cuyo (06/C440 and 06/C454).

References

[1] H. Trinkaus, B.N. Singh, J. Nucl. Mater. 323 (2003) 229–242.
[2] H. Ullmaier, Nucl. Fusion 24 (1984) 1039–1083.
[3] S.K. Das, M. Kaminsky, Radiation blistering in metals and alloys, in: Proc. of Symposium of Radiation Effects on Solids Surfaces, Argonne National Laboratory, Chicago, 1975.
[4] H. Shinno, H. Shiraishi, R. Watanabe, H. Kamitsubo, I. Kohno, T. Shikata, J. Nucl. Mater. 97 (1981) 291–299.
[5] K. Yutani, H. Kishimoto, R. Kasada, A. Kimura, J. Nucl. Mater. 367–370 (2007) 423–427.
[6] N. Kamigaki, S. Furuno, K. Hojou, K. Ono, E. Hashimoto, K. Izui, T. Kino, J. Nucl. Mater. 191–194 (1992) 1214–1218.
[7] S. Furuno, K. Hojou, H. Otsu, K. Izui, N. Kamigaki, K. Ono, T. Kino, Microsc. Microanal. Microstruct 4 (1993) 323–330.
[8] E. Ruedl, O. Gautsch, E. Staroste, J. Nucl. Mater. 62 (1976) 63–72.
[9] G. Feldmann, P.F.P. Fichtner, F.C. Zawislak, Acta Mater. 52 (2004) 693–703.
[10] D. Mitlin, V. Radmilovic, J.W. Morris, U. Dahmen, Metall. Mater. Trans A 34 (2003) 735–742.
[11] http://www.srim.org, Ziegler J.F..
[12] R.F. Egerton, R. McLeod, F. Wang, M. Malac, Ultramicroscopy 110 (2010) 991–997.
[13] H. Trinkaus, Rad. Eff. 78 (1983) 189–211.
[14] K. Ono, M. Inoue, T. Kino, S. Furuno, K. Izui, J. Nucl. Mater. 133–134 (1985) 477–481.
[15] G.J. Thomas, Rad. Eff. 78 (1983) 37–51.

[16] N.F. Carnahan, K.E. Starling, J. Chem. Phys. 51 (1969) 635–636.
[17] I.R. Berarley, D.A. MacInnes, J. Nucl. Mater. 95 (1980) 239–252.
[18] W. Jäger, R. Manzke, H. Trinkaus, G. Crecelius, R. Zeller, J. Nucl. Mater. 111–112 (1982) 674–680.
[19] K. Farrel, J.T. Houston, J. Nucl. Mater. 83 (1979) 57–66.
[20] P.B. Johnson, R.W. Thomson, K. Reader, J. Nucl. Mater. 273 (1999) 117–129.
[21] M.A. Nguyen, M.O. Ruault, F. Fortuna, Adv. Nat. Sci. Nanosci. Nanotechnol 3 (2012) 01501.
[22] D. Niebieskikwiat, E.E. Kaul, G.R. Pregliasco, J.E. Gayone, O. Grizzi, E.A. Sánchez, Nucl. Instrum. Methods Phys. Res. B193 (2002) 305–311.
[23] M. Braun, J.L. Whitton, B. Emmoth, J. Nucl. Mater. 85–86 (1979) 1091–1094.
[24] S.K. Das, M. Kaminsky, G. Fenske, J. Nucl. Mater. 76–77 (1978) 215–220.